1,3-Thiazole as Suitable Antenna Ligand for Lanthanide Photoluminescence in $[LnCl_3(thz)_4]\cdot 0.5thz$, Ln = Sm, Eu, Gd, Tb, Dy

Nicole Dannenbauer[a], Ana Kuzmanoski[b], Claus Feldmann[b], and Klaus Müller-Buschbaum[a]

[a] Julius-Maximilians-University, Institute for Inorganic Chemistry, Am Hubland, 97074 Würzburg, Germany

[b] Karlsruhe Institute of Technology (KIT), Institute for Inorganic Chemistry, Engesserstraße 15, 76131 Karlsruhe, Germany

Reprint requests to Klaus Müller-Buschbaum. Fax: +49 931 31-84785.
E-mail: k.mueller-buschbaum@uni-wuerzburg.de

Z. Naturforsch. **2014**, *69b*, 255 – 262 / DOI: 10.5560/ZNB.2014-3292
Received October 29, 2013

The series of luminescent monomeric lanthanide thiazole complexes $[LnCl_3(thz)_4]\cdot 0.5thz$ (Ln = Sm, Eu, Gd, Tb, Dy; thz = 1,3-thiazole) has been synthesised and characterised by powder and single-crystal X-ray diffraction, IR and photoluminescence spectroscopy, DTA/TG as well as elemental analysis. The colourless compounds exhibit photoluminescence in the visible region with varying quantum efficiencies up to $QY = 48\,\%$ for $[TbCl_3(thz)_4]\cdot 0.5thz$. Both, the lanthanide ions as well as the thiazole ligand contribute to the luminescence. Excitation can be achieved *via* intra-4f transitions and by exciting the ligand, emission is observed mainly from the lanthanide ions again by 4f transitions. Thiazole can transfer energy to the lanthanide ions, which further feeds the lanthanide emission by an efficient antenna effect even at room temperature. The lanthanide ions show pentagonal-bipyramidal coordination by three chloride anions and four N atoms of 1,3-thiazole, which leads to a strong $^5D_0 \rightarrow {}^7F_4$ transition for europium. Significant differences arise as compared to thiophene complexes because no sulphur atom is involved in the metal coordination, as the thiazole ligand is solely coordinated *via* its nitrogen function.

Key words: Thiazole, Lanthanides, Luminescence, Energy Transfer

Introduction

Due to the sharp emission lines and therefore a good colour quality, there is a growing interest in lanthanide complexes as candidates for applications in the fields of electronics [1, 2] and photonics [3 – 5]. However, the direct light absorption of trivalent lanthanide ions is usually low due to the parity forbidden character of *intra*-4f transitions (smaller than $\varepsilon = 10\,L\,mol^{-1}\,cm^{-1}$) [6]. The weak absorption coefficients can be circumvented by energy transfer from an antenna, mostly organic "chromophores", to Ln^{3+} centres. Energy migration from ligand to metal implies Laporte- and spin-allowed ligand-centred absorption, which can be followed by intersystem crossing in the ligand and energy transfer to the metal ions, and ends up in metal-centred emission. The efficiency of the antenna effect can be maximised if excited energy states of the ligand are higher and close to the energy levels of excited states of the lanthanide ions [7, 8]. The latter show luminescence with emissions spanning over the entire electromagnetic spectrum from the UV (Gd^{3+}) to the visible (Sm^{3+}, Eu^{3+}, Tb^{3+}, Dy^{3+}) and near-infrared (Nd^{3+}, Er^{3+}, Yb^{3+}) regions [9]. Remarkable investigations on luminescent lanthanide complexes were carried out on ligands like terphenyls [10], β-diketones [11], cryptands [12], quinoline derivates [13], and carboxylates [14]. As the work on thiazole complexes $[LnCl_3(thz)_4]\cdot 0.5thz$ (Ln = Sm, Eu, Gd, Tb, Dy; thz = 1,3-thiazole), presented here, shows, small heterocyclic five-membered aromatic ligands like 1,3-thiazole can also exhibit antenna effects, effectively supporting the lanthanide luminescence. Recently, a first lanthanide thiazole complex has been reported, $[Pr_4Cl_{10}(OH)_2(thz)_8(H_2O)_2][Pr_2Cl_6(thz)_8]$ [15],

which already gave hints on the presence of anhydrous secondary phases. Now, the synthesis of $[LnCl_3(thz)_4]\cdot 0.5thz$ confirms the existence of such anhydrous complexes.

Results and Discussion

Crystal and molecular structure

The reaction of anhydrous $LnCl_3$ (Ln = Sm, Eu, Gd, Tb, Dy) with 1,3-thiazole with no further solvents yields colourless crystals of the formula $[LnCl_3(thz)_4]\cdot 0.5thz$ (Ln = Sm, Eu, Gd, Tb, Dy; thz = 1,3-thiazole). The structures of $[LnCl_3(thz)_4]\cdot 0.5thz$ (Ln = Sm, Eu, Gd, Tb, Dy) were determined on single crystals of **1** (Sm) and **4** (Tb), which are isotypic to **2** (Eu), **3** (Gd) and **5** (Dy), as proven by powder X-ray diffraction including indexing of the diffractograms of the latter compounds. Refinements of the lattice parameters were carried out on the diffractograms using a series of reflections with the best possible resolution, and all led to monoclinic unit cells. The isotypic series of $[LnCl_3(thz)_4]\cdot 0.5thz$ (**1**–**5**) crystallises in the monoclinic space group *Pn* with $Z = 2$ (Table 1 gives crystallographic data for **1** and **4**). Single crystals are formed as racemic twins with a varying ratio of the twin individuals. The structure is non-centrosymmetric owing to the orientation of the complexes in the crystal structure. *Ln* atoms exhibit a distorted pentagonal-bipyrimidal coordination polyhedron (Fig. 1) of four nitrogen atoms of four different thiazole ligands in the equatorial plane, and three chlorine atoms, two of them occupying the axial positions. Distortion derives from the differences in *Ln*–Cl and *Ln*–N distances resulting in the largest deviation from the ideal polyhedron for the axial Cl–*Ln*–Cl angle $(170.2(1)^\circ$ for Sm in **1** and $171.3(1)^\circ$ for Tb in **4**). As expected, the axial interatomic distances Sm–Cl (2.663(1) – 2.669(1) Å) are shorter than the equatorial Sm–Cl distance with 2.680(1) Å. They correspond with $[Sm(ntb)Cl_3]$ (ntb = tris(benzimidazol-2-ylmethyl)amine), showing interatomic distances in the range of 2.674 – 2.713 Å [16]. The Sm–N distances in the monomers of $[SmCl_3(thz)_4]\cdot 0.5thz$ range from 2.549(2) to 2.589(2) Å and match with known Sm–N distances

Table 1. Crystal structure data for **1** and **4**.

	1	**4**
Empirical formula	$Sm_2Cl_6C_{27}H_{27}N_9S_9$	$Tb_2Cl_6C_{27}H_{27}N_9S_9$
M_r	1279.60	1296.73
Crystal size, mm^3	$0.05 \times 0.09 \times 0.18$	$0.07 \times 0.15 \times 0.28$
Crystal system	monoclinic	monoclinic
Space group	*Pn*	*Pn*
a, Å	9.0078(6)	9.053(2)
b, Å	15.3972(10)	15.581(3)
c, Å	16.8685(11)	16.813(3)
β, deg	102.40(2)	102.25(3)
V, Å^3	2285.0(3)	2317.6(8)
Z	2	2
$D_{calcd.}$, g cm^{-3}	1.86	1.86
μ (MoK_α), cm^{-1}	3.3	3.8
F (000), e	1251	1263
hkl range	$-12 \le h \le +12$	$-11 \le h \le +11$
	$-21 \le k \le +21$	$-20 \le k \le +19$
	$-23 \le l \le +23$	$-21 \le l \le +21$
Refl. measured/unique/R_{int}	33 657/12 404/0.026	34 625/10 180/0.049
Param. refined	484	484
$R(F)/wR(F^2)$[a] (all refls.)	0.0226/0.0421	0.0339/0.0720
x(Flack) (BASF of racemic twin refinement)	0.088(4)	0.49(2)
GoF (F^2)[a]	0.9707	1.0402
$\Delta\rho_{fin}$ (max/min), e Å^{-3}	1.63/−0.76	1.63/−0.53

[a] $R(F) = \Sigma||F_o| - |F_c||/\Sigma|F_o|$; $wR(F^2) = [\Sigma w(F_o^2 - F_c^2)^2/\Sigma w(F_o^2)^2]^{1/2}$, $w = [\sigma^2(F_o^2) + (AP)^2 + BP]^{-1}$, where $P = (\mathrm{Max}(F_o^2, 0) + 2F_c^2)/3$ and A and B are constants adjusted by the program; GoF = $S = [\Sigma w(F_o^2 - F_c^2)^2/(n_{obs} - n_{param})]^{1/2}$, where n_{obs} is the number of data and n_{param} the number of refined parameters.

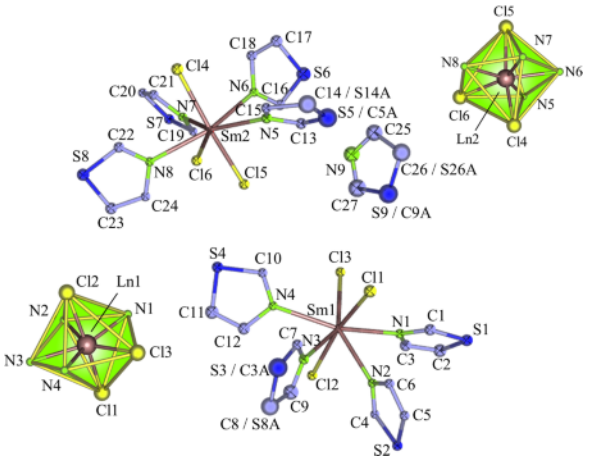

Fig. 1 (colour online). Molecular structure of $[LnCl_3(thz)_4]\cdot 0.5thz$ with displacement ellipsoids at the 50% probability level for *Ln* = Sm, **1** (C8/S3, C14/S5 and C26/S9 isopositionally disordered). Distorted pentagonal-bipyramidal coordination spheres of the Ln^{3+} ions in **1**–**5**, shown for *Ln* = Sm (**1**).

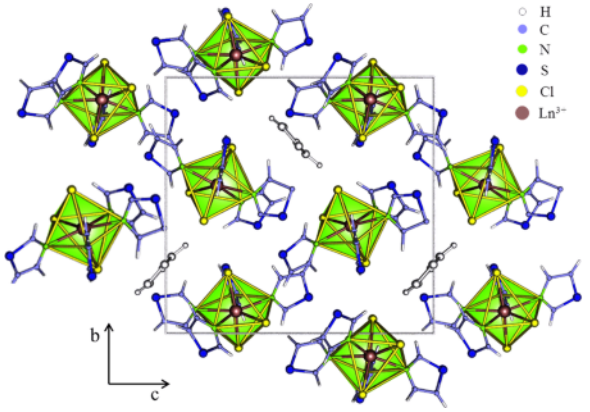

Fig. 2 (colour online). Crystal structure of $[LnCl_3(thz)_4]\cdot 0.5thz$ projected along [100] with coordination polyhedra, here shown for *Ln* = Sm (**1**).

in $[Sm(mtp)Cl_2(N\text{-MeIm})_2(THF)]\cdot 2PhMe$ (mtp = 2,2′,4,4′,6,6′-hexamethyl-*m*-terphenyl, *N*-MeIm = N-methylimidazole, THF = tetrahydrofuran, PhMe = toluene) [17] and $[Sm(N\text{-MeIm})_8]I_3$ (2.505–2.596 Å) [18] The interatomic distances for the analogous complex $[TbCl_3(thz)_4]\cdot 0.5thz$ are also in good agreement with distances of related structures of $[Tb(tpa)Cl_3]$, tpa = tris[(2-pyridyl)methyl]amine and $[\{(tp)_2Tb(\mu\text{-}N_3)\}_4]\cdot 6CH_2Cl_2$, tp = hydrotris(pyrazol-1-yl)borate [19, 20] and range for Tb–Cl from 2.612(1)–2.676(1) and for Tb–N from 2.521(4)–2.575(4) Å. Fig. 1 shows the structure of the crystallographically independent complexes of $[LnCl_3(thz)_4]\cdot 0.5thz$ for samarium. Apparently, the sulphur atom of the 1,3-thiazole ligand is not coordinating but only the nitrogen function. 1,3-Thiazole acts as chemical scissor, cutting the $LnCl_3$ structure down to monomers by adding itself as a donor ligand. The complete crystal structure of $[LnCl_3(thz)_4]\cdot 0.5thz$ (*Ln* = Sm, Eu, Gd, Tb, Dy) further contains one equivalent of non-coordinating thiazole, as shown in Fig. 2.

Photoluminescence spectroscopy of $[LnCl_3(thz)_4]\cdot 0.5thz$ (Ln = Sm, Eu, Gd, Tb, Dy)

The series of the complexes $[LnCl_3(thz)_4]\cdot 0.5thz$ (*Ln* = Sm, Eu, Gd, Tb, Dy; **1**–**5**) reveals photoluminescence properties subsequent to excitation with UV light. The emissions of all compounds are in the visible region and show the typical emission colours for each ion (given in parentheses): Sm^{3+} (salmon red), Eu^{3+} (red), Tb^{3+} (green) and Dy^{3+} (yellow). The Gd^{3+} complex exhibits a weak blue emission. The normalised excitation and emission spectra recorded at room temperature are shown in Figs. 3 and 4. The emission spectra exhibit sharp $4f$-$4f$ transitions for all Ln^{3+} ions, except for Gd^{3+}.

Sm^{3+} emissions in **1** are observed at 564 (green), 597 (orange-red), 648 (red) and 707 (red) nm, and are assigned to the electronic transitions $^4G_{5/2} \rightarrow {}^6H_{J/2}$ ($J = 5, 7, 9, 11$). Remarkably, the emission intensity is

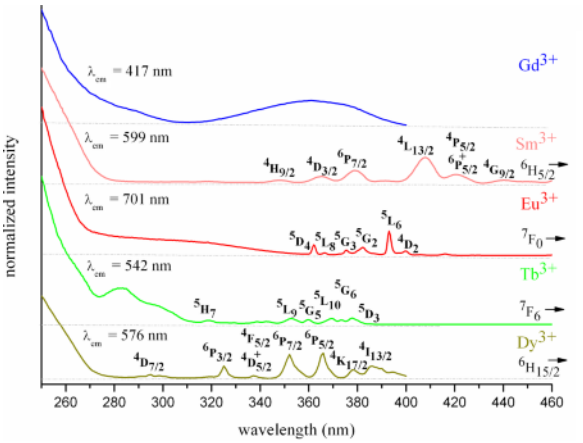

Fig. 3 (colour online). Normalised solid-state excitation spectra of $[LnCl_3(thz)_4]\cdot 0.5thz$ for *Ln* = Sm, Eu, Gd, Tb, Dy (**1**–**5**) at room temperature.

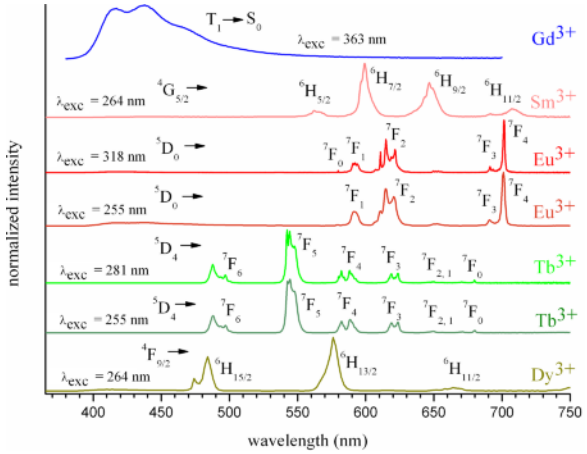

Fig. 4 (colour online). Normalised solid-state emission spectra of $[Ln\mathrm{Cl_3(thz)_4}]\cdot 0.5\mathrm{thz}$ for $Ln = $ Sm, Eu, Gd, Tb, Dy (**1**–**5**) at room temperature.

quite strong for Sm^{3+} as it is supported by the antenna effect of the ligand.

The emission spectrum of the Eu^{3+} complex **2** exhibits the five characteristic emission lines of the metal ion. They can be assigned to $^5D_0 \rightarrow {}^7F_n$ ($n = 1$, 2, 3, 4, 5) transitions, respectively. The $^5D_0 \rightarrow {}^7F_4$ emissions at 702 and 613 nm ($^5D_0 \rightarrow {}^7F_2$) are the strongest, the latter is also called a hypersensitive transition [21, 22]. The ratio of the intensities of the electric dipole to the magnetic dipole transitions of 3.49 for $I(^5D_0 \rightarrow {}^7F_2)/I(^5D_0 \rightarrow {}^7F_1)$ indicates that the Eu^{3+} centres have a coordination environment of low symmetry [23]. Moreover, the presence of a sharp emission line for the $^5D_0 \rightarrow {}^7F_0$ transition at 579 nm suggests the presence of a single chemical environment of one point group symmetry for Eu^{3+} [24]. This is consistent with the result of the single-crystal X-ray analysis. It is remarkable that the emission to the $^7F_4$ state is the strongest in intensity. This observation is in correspondence with other five-fold and seven-fold nitrogen/chlorine coordinations and has been observed for $Na_9[EuW_{10}O_{36}]\cdot 14H_2O$ [25], $^3_\infty[EuCl_3(1,3\text{-}Ph(CN)_2)]$ [26] or $^2_\infty[Eu_2Cl_6(bipy)_3]\cdot 2(bipy)$ [27, 28], 1,3-Ph(CN)$_2$ = 1,3-benzodintrile, bipy = 4,4′-bipyridine, and explained by a strong ligand- and temperature polarisability-dependent dynamic coupling (DC) effect. Usually, the $^5D_0 \rightarrow {}^7F_2$ transition has the highest intensity, while $^5D_0 \rightarrow {}^7F_4$ is rather weak. An enhanced intensity of the latter can be a consequence of the intensity parameters Ω_λ in a highly polarisable environment [25, 26].

The Tb^{3+}-containing compound **4** shows the typical transitions between the excited $^5D_4$ state and the $^7F_{6-0}$ levels of the Tb^{3+} septet. The highest intensity is found for the transition $^5D_4 \rightarrow {}^7F_5$ at 542 nm, as expected for a Tb^{3+} emission [7]. All seven transitions are present at 487, 545, 589, 623, 649, 669, and 679 nm (Table 2).

Furthermore, for $[DyCl_3(thz)_4]\cdot 0.5\mathrm{thz}$ (**5**) three emission lines at 485, 576 and 664 nm are corresponding with the first excited $^4F_{9/2}$ state, the $^6H_{13/2}$ state and the $^6H_{15/2}$ level of the ground state of Dy^{3+}. Again, the antenna effect of the ligand increases the overall intensity of the dysprosium emission.

Table 2. Excitation and emission wavelengths (in nm) of the transitions of $[Ln\mathrm{Cl_3(thz)_4}]\cdot 0.5\mathrm{thz}$ ($Ln = $ Sm, Eu, Tb, Dy).

	Intra-4*f* excitation transitions		
Sm^{3+}	$^6H_{5/2} \rightarrow$	$^4H_{9/2}$, $^4D_{3/2}$, $^6P_{7/2}$, $^4L_{13/2}$, $^6P_{5/2}$+$^4P_{5/2}$, $^4G_{9/2}$	347, 364, 379, 408, 420, 440
Eu^{3+}	$^7F_0 \rightarrow$	$^5D_4$, $^5L_8$, $^5G_3$, $^5G_2$, $^5L_6$, $^5D_2$	362, 365, 375, 382, 393, 400
Tb^{3+}	$^7F_6 \rightarrow$	$^5H_7$, $^5L_9$, $^5G_5$, $^5L_{10}$, $^5G_6$, $^5D_3$	318, 352, 360, 369, 374, 378
Dy^{3+}	$^6H_{15/2} \rightarrow$	$^4D_{7/2}$, $^6P_{3/2}$, $^4F_{5/2}$+$^4D_{5/2}$, $^6P_{7/2}$, $^6P_{5/2}$, $^4K_{17/2}$, $^4I_{13/2}$	295, 325, 337, 352, 366, 378, 386
	Intra-4*f* emission transitions		
Sm^{3+}	$^4G_{5/2} \rightarrow$	$^6H_{5/2} - {}^6H_{11/2}$	564, 597, 648, 707
Eu^{3+}	$^5D_0 \rightarrow$	$^7F_0 - {}^7F_6$	579, 593, 615, 652, 702
Tb^{3+}	$^5D_4 \rightarrow$	$^7F_6 - {}^7F_0$	487, 545, 589, 623, 649, 669, 679
Dy^{3+}	$^4F_{9/2} \rightarrow$	$^6H_{11/2} - {}^6H_{9/2}$	485, 576, 664

Although the main light absorption is observed for the thiazole ligand, and to lesser extent for the lanthanide ions, almost no ligand-based emission is observed for $[LnCl_3(thz)_4]\cdot 0.5thz$ (Ln = Sm, Eu, Tb, Dy), indicating a ligand-to-metal energy transfer process. Thus, 1,3-thiazole acts as a suitable antenna for sensitisation of the lanthanide-based emission according to the following steps: (1) absorption of light by the ligand in a transition $S_n \leftarrow S_0$, (2) ISC (intersystem crossing) from singlet (S) to triplet (T) levels of the ligand and (3) excitation energy transfer to the lanthanide ions. It seems that a suitable energy gap between excited $4f$ states of $Sm^{3+}/Eu^{3+}/Tb^{3+}/Dy^{3+}$ at about 25 000 – 26 000 cm^{-1} (Sm^{3+}: $^5L_{15/2} \sim 25\,650$; Eu^{3+}: $^5L_6 \sim 25\,400$; Tb^{3+}: $^5D_3 \sim 26\,273$; Dy^{3+}: $^4I_{13/2} \sim 25\,900$ cm^{-1}) [29, 30], and the lowest predicted triplet T_1 level of 1,3-thiazole (26 045 cm^{-1}) [31] leads to an effective sensitisation *via* equal energy levels, while energy back transfer processes are avoided by reduction of the energy on the lanthanide ions to the emissive states of $Sm^{3+}/Eu^{3+}/Tb^{3+}/Dy^{3+}$ ($^4G_{5/2} \sim 17\,900$; $^5D_0 \sim 17\,500$; $^5D_4 \sim 20\,500$; $^4F_{9/2} \sim 21\,000$ cm^{-1}).

The emission spectrum of the gadolinium complex $[GdCl_3(thz)_4]\cdot 0.5thz$ (**3**) is a good candidate to evaluate the behaviour of 1,3-thiazole in the series of complexes as it exhibits no $4f$-$4f$ emission but a distinct ligand-based $T_1 \rightarrow S_0$ emission process from 400 – 540 nm, proving the relevance of the triplet states present in thiazole.

The excitation spectra for $[LnCl_3(thz)_4]\cdot 0.5thz$ (Ln = Sm, Eu, Tb, Dy) display a strong ligand $S_n \leftarrow S_0$ excitation band in the UV range starting outside the observable range of our spectrometer and ranging to 280 nm. Furthermore, triplet excitation with a maximum of 363 nm is observed for Gd^{3+}. In addition, typical weak $4f$-$4f$ transitions for the trivalent lanthanides Sm, Eu, Tb and Dy, and except for Gd, are observed, for example for Eu^{3+} at 362, 365, 375, 382, 393, and 400 nm (corresponding transitions for the Ln^{3+} ions are listed in Table 2). This confirms the sensitisation of the Ln^{3+} emission by the ligand as well as by weak direct $4f$ excitation. The ratio between light absorption of the lanthanide ion and the ligand excitation gives an insight into the efficiency of the antenna effect. This is most prominent for the case of Tb^{3+}, in which the intensity of the $4f$-excited Tb^{3+}-centred emission is rather low compared to the excitation triggered by the antenna effect. In order to further evaluate the efficiency of the energy transfer process, emission was also recorded for several different ligand-based excitation wavelengths (see for europium and terbium in Fig. 4). Whereas the energy transfer is complete for excitation wavelengths that give weaker excitation, remnants of the ligand emission are present if the strong light uptake of the $S_n \leftarrow S_0$ transition is used (*e. g.* between 250 – 265 nm). Although the energy transfer is still active and leads to brighter emission, not all of the absorbed energy can be utilised in the energy transfer.

In order to quantify the luminescence properties of the complexes in the visible region, we also determined the quantum yields QY of the compounds $[LnCl_3(thz)_4]\cdot 0.5thz$ (Ln = Sm, Eu, Tb). For antenna effect-based excitation of the Ln^{3+} emission, the observed quantum yield for Tb^{3+} is 25(3) % and for Eu^{3+} 11(2) % (determined at $\lambda_{exc} = 254$ nm). In comparison, the quantum yield is almost twice as high for longer excitation wavelengths directly deriving from $4f$-$4f$ transitions on the Ln^{3+} ions (46(3) % for Tb^{3+}, determined at $\lambda_{exc} = 378$ nm; 18(2) % for Eu^{3+}, determined at $\lambda_{exc} = 393$ nm). In contrast, samarium shows a much less effective energy transfer, represented by a QY of below 5 %, if excited *via* the ligand at 254 nm. While the quantum yield quantifies the efficiency of the luminescence processes, including absorption, energy transfer and emission, the number of photons absorbed/emitted per time unit also has to be considered in view of the brightness of emission. Thus, $[SmCl_3(thz)_4]\cdot 0.5thz$ can show bright salmon-red emission due to allowed and intense absorption, although its quantum yield is low. These findings illustrate the necessity to evaluate quantum yield, light uptake and energy transfer in order to classify a material.

Thermal investigation

Simultaneous DTA and TGA investigations were conducted in inert gas to study the thermal stability of the title complexes $[LnCl_3(thz)_4]\cdot 0.5thz$ (Ln = Sm–Dy, **1**–**5**). The results of DTA/TG match for the five compounds and are depicted exemplarily for crystalline **5** (Dy) in the temperature range of 25 – 750 °C in Fig. 5. The heat flow shows no less than seven signals of which four are related to mass losses. The initial mass loss is tied up with two endothermic signals 1 and 2 (80 °C, mass loss: 19.5 %) and can be associated with release of the non-coordinating thiazole as well as one equivalent of coordinated thiazole (theoretical mass loss: 19.5 %). The remaining product decomposes sub-

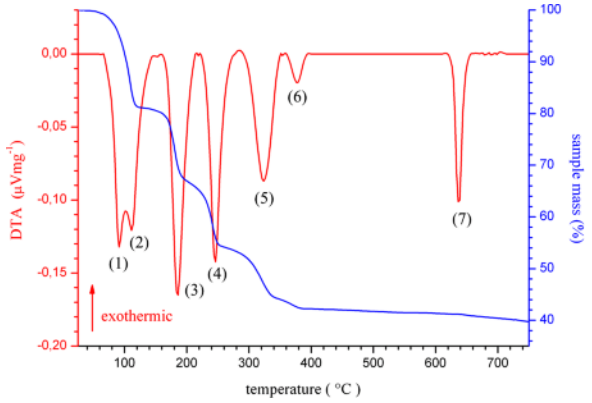

Fig. 5 (colour online). DTA/TG investigation of $[LnCl_3(thz)_4]\cdot 0.5thz$ for $Ln = Dy$ (**5**).

sequently giving endothermic signals 3 (170 °C) and 4 (225 °C) with a mass loss of 13.5 and 13 %, respectively, that can be identified as a release of another equivalent of coordinated thiazole in each step (theoretical mass loss for each step: 13 %). The remaining coordinated thiazole equivalent is lost thereafter (mass loss of 13 %), for 5 at 300 °C and for 6 at 370 °C. The residual mass of 42 % coincides approximately with the theoretical value of $DyCl_3$ (42 %). This observation may be associated with reformation of crystalline $DyCl_3$. The approval of the latter interpretation is supported by the endothermic signal 7 at 630 °C, which roughly corresponds with the theoretical melting point of $DyCl_3$ (654 °C) [32].

Conclusion

Thiazole complexes $[LnCl_3(thz)_4]\cdot 0.5thz$ of the lanthanide trichlorides of samarium, europium, gadolinium, terbium, and dysprosium were synthesised in sealed ampoules by direct reaction without further solvents. Spontaneous reaction is observed already at room temperature, giving the first anhydrous thiazole complexes of the lanthanides. The products are luminescent in the visible region, exhibiting typical $4f$-$4f$ emission of the trivalent lanthanide ions, except for gadolinium and europium. Whereas Eu^{3+} marks the exception of a strong emission into the $^7F_4$ state, related to the seven-fold coordination and a ligand- and temperature polarisability-dependent dynamic coupling (DC) effect, Gd^{3+} shows no $4f$ emission, but broad ligand bands. The gadolinium complex proved to be a suitable candidate to validate the presence of excited triplet states that are likely to take part in the energy transfer from the ligand to the metal ions for the other lanthanides. Their emission is supported by an antenna effect of the thiazole ligand leading to a remarkably strong $4f$ emission for Sm^{3+} and Dy^{3+}. In addition, the excitation wavelength-dependent quantum yields of the solid compounds were determined, ranging up to 48 % for Tb^{3+}.

Experimental Section

All operations were performed under inert conditions (argon atmosphere) using vacuum line, Schlenk and glove box (MBraun, LabMaster SP and Innovative Technology, Pure Lab) and Duran® ampoule techniques. The infrared spectra were recorded on KBr pellets on a Thermo Nicolet 380 FT-IR spectrometer in transmission mode using the OMNIC 32 software. Luminescence spectra were recorded with a Horiba Jobin Yvon Spex Fluorolog 3 spectrometer equipped with a 450 W Xe lamp, double grated excitation and emission monochromators and a PMT at r. t., and the FLUORESSENCE software.

The quantum yield was also recorded using a photoluminescence spectrometer Horiba Jobin Yvon Spex Fluorolog 3, equipped with a 450 W xenon lamp, double monochromators for excitation and emission, an integrating sphere (Ulbricht sphere) and a photomultiplier as the detector. For excitation wavelengths > 330 nm, the absolute quantum yield was determined according to Friend [33]. First the diffuse reflection of the sample was determined at a certain excitation wavelength. Second, the emission was measured under excitation at the same wavelength. Integration of the reflected and emitted photons by use of the Ulbricht sphere resulted in the absolute quantum yield. Corrections were made accounting for the spectral power of the excitation source, the reflection behaviour of the Ulbricht sphere, and the sensitivity of the detector. For excitation wavelengths < 330 nm, the reflectivity of the Ulbricht sphere starts to be perceptibly below 100 % resulting in a less precise determination of the absolute quantum yield. Therefore, the relative quantum yield was determined by comparison to a reference phosphor with a defined quantum yield. Here, Y_2O_3:Eu (5 mol-% Eu, YO*X*) and $LaPO_4$:Ce,Tb (45 mol-% Ce, 15 mol-% Tb, LAP) were used as technical reference phosphors that exhibit a quantum yield of 80 % (red emission) [34] and 86 % (green emission) [35], respectively, at $\lambda_{exc} = 254$ nm.

The powder samples were prepared in Lindemann glass capillaries ($\varnothing = 0.3$ mm), and the powder diffractograms were recorded on a Bruker D8 Discover Da Vinci in transmission geometry with a focusing Göbel mirror and LynxEye detector with CuK_α radiation ($\lambda = 1.54056$ Å). The thermal properties of the bulk substance were investigated by simul-

taneous DTA/TG (Netzsch STA 409, Proteus Software), using 25 mg of sample. The sample was kept under an inert gas atmosphere (50 % Ar and 50 % N_2) and heated from 25 to 750 °C with a heating rate of 10 °C min. Elemental analysis for C, H, N, and S was performed with a Vario EL (Elementar Analysensysteme GmbH).

*Synthesis of [LnCl$_3$(thz)$_4$]·0.5thz (Ln = Sm, Eu, Gd, Tb, Dy) **1–5***

*Ln*Cl$_3$ (0.3 mmol, (*Ln*: Sm = 77.0, Eu = 77.5, Gd = 79.0, Tb = 79.5, Dy = 80.5 mg) and 1,3-thiazole (C_3H_3NS, 1.5 mmol, 127.5 mg) were sealed in an evacuated Duran® glass ampoule. Highly reflecting transparent crystals are moisture sensitive and resulted from a reaction of both components at room temperature within 6 h. Reaction starts immediately upon contact of the reagents. Ligand excess was removed by evaporation under vacuum. Yield: Sm = 87 (167 mg), Eu = 92 (176 mg), Gd = 88 (172 mg), Tb = 89 (175 mg), Dy = 90 (176 mg) %. – IR (KBr, cm^{-1}): Sm (**1**): ν = 3403 (w), 3083 (m), 1653 (m), 1540 (m), 1495 (m), 1382 (m), 1312 (m), 1243 (m), 1135 (w), 1051 (s), 905 (s), 872 (m), 830 (m), 818 (m), 754 (m), 726 (w), 615(s), Eu (**2**): ν = 3403 (w), 3093 (m), 1495 (m), 1381 (m), 1311 (s), 1246 (m), 1119 (m), 1050 (s), 904 (s), 872 (m), 831 (m), 821 (m), 749 (m), 726 (m), 615(s); Gd (**3**): ν = 3341 (w), 3080 (m), 1631 (w), 1495 (m), 1381 (m), 1310 (s), 1243 (m), 1120 (m), 1047 (s), 904 (s), 873 (m), 812 (m), 779 (w), 744 (m), 611(s); Tb (**4**): ν = 3403 (w), 3089 (m), 1496 (m), 1381 (m), 1311 (s), 1243 (m), 1121 (m), 1047 (m), 905 (s), 874 (m), 849 (w), 812 (s), 744 (m), 726 (m), 613(s); Dy (**5**): ν = 3403 (w), 3090 (m), 1497 (m), 1381 (m), 1311 (s), 1243 (w), 1121 (m), 1049 (m), 905 (s), 873 (m), 813 (m), 744 (m), 726 (w), 613(s). – Anal. for $Sm_2Cl_6C_{27}H_{27}N_9S_9$ (1279.60): calcd. C 25.34, H 2.13, N 9.85, S 22.55; found C 25.45, H 2.29, N 9.97, S 22.29; $Eu_2Cl_6C_{27}H_{27}N_9S_9$ (1282.81): calcd. C 25.28, H 2.12, N 9.83, S 22.50; found C 25.83, H 2.24, N 9.89, S 22.38; $Gd_2Cl_6C_{27}H_{27}N_9S_9$ (1293.38): calcd. C 25.07, H 2.10, N 9.75, S 22.31; found C 24.56, H 2.43, N 9.27, S 21.97; $Tb_2Cl_6C_{27}H_{27}N_9S_9$ (1296.73): calcd. C 25.01, H 2.10, N 9.72, S 22.26; found C 25.32, H 2.13, N 9.71, S 22.73; $Dy_2Cl_6C_{27}H_{27}N_9S_9$ (1303.88): calcd. C 24.87, H 2.09, N 9.67, S 22.13; found C 25.19, H 2.43, N 9.77, S 22.90.

X-Ray structure determinations

Single crystals of [*Ln*Cl$_3$(thz)$_4$]·0.5thz (*Ln* = Sm, Tb, **1**, **4**) were selected for X-ray investigations and mixed with high-viscosity perfluorinated ether (99.9 %, ABCR). Data collection for the compounds is carried out for **4** (Tb) on a Bruker AXS Smart Apex I CCD diffractometer with graphite monochromator at 173 K (MoK_α radiation; λ = 0.71073 Å) and for **1** (Sm) on an Enraf Nonius & Bruker AXS ApexII CCD diffractometer with graphite monochromator at 100 K (MoK_α radiation; λ = 0.71073 Å), using the Bruker AXS SMART Software package [36]. Further data processing used XPREP [37]. The structures were solved by Direct Methods using SHELXS-97 [38] and refined using SHELXL-97 [38] on the graphical platform OLEX2 [39]. Integrity of symmetry was checked using PLATON [40]. For both compounds, all non-hydrogen atoms were refined anisotropically by least-squares methods, and all hydrogen atoms were added with geometrical constraints regarding their positions. Both isotypic compounds crystallise as racemic twins in the monoclinic space group *Pn*. The terminal coordination of the thiazole ligands gives them a certain freedom regarding the positions of the opposite C and S atoms, represented by a lack of order of ring positions 3 and 4. This was described by refinement of mixed positions for C and S in an isopositional disorder of the atomic positions in three thiazole rings: (for [SmCl$_3$(thz)$_4$]·0.5thz (**1**): (N3-C7-C8/S8A-S3/C3A-C9), (N5-C13-C14/S14A-S5/C5A-C15) and (N9-C25-C26/S26A-S9/C9A-C27) (for [TbCl$_3$(thz)$_4$]·0.5thz (**4**): (N3-C7-C8/S8A-S3/C3A-C9), (N8-C22-C23/S23A-S8/C8A-C24) and (N9-C25-C26/S26A-S9/C9A-C27)).

CCDC 969259 for Sm (**1**) and 969260 for Tb (**4**) contain the supplementary crystallographic data for this paper. These data can be obtained free of charge from The Cambridge Crystallographic Data Centre *via* www.ccdc.cam.ac.uk/data_request/cif.

[1] A. J. Kenyon, *Prog. Quantum Electron.* **2002**, *26*, 225 – 284.
[2] Y. Chen, W. Su, M. Bai, J. Jiang, X. Li, Y. Liu, L. Wang, S. Wang, *J. Am. Chem. Soc.* **2005**, *127*, 15700 – 15701.
[3] Y. Hasegawa, Y. Wada, S. Yanagida, *J. Photochem. Photobiol. C* **2004**, *5*, 183 – 202.
[4] N. T. Kalyani, S. J. Dhoble, *Renewable Sustainable Energy Rev.* **2012**, *16*, 2696 – 2723.
[5] J.-C. G. Bünzli, S. Comby, A.-S. Chauvin, C. D. B. Vandevyver, *J. Rare Earths* **2007**, *25*, 257 – 274.
[6] J.-C. G. Bünzli, C. Piguet, *Chem. Soc. Rev.* **2005**, *34*, 1048 – 1077.
[7] K. Binnemans, *Chem. Rev.* **2009**, *109*, 4283 – 4374.
[8] S. V. Eliseeva, J.-C. G. Bünzli, *Chem. Soc. Rev.* **2010**, *39*, 189 – 227.
[9] J.-C. G. Bünzli, *Chem. Rev.* **2010**, *110*, 2729 – 2755.

[10] S. Petoud, J.-C. G. Bünzli, K. J. Schenk, C. Piguet, *Inorg. Chem.* **1997**, *36*, 1345 – 1353.
[11] N. M. Shavaleev, R. Scopelliti, F. Gumy, J.-C. G. Bünzli, *Eur. J. Inorg. Chem.* **2008**, 1523 – 1529.
[12] N. Sabbatini, M. Guardigli, J. M. Lehn, *Coord. Chem. Rev.* **1993**, *123*, 201 – 228.
[13] M. Albrecht, O. Osetska, J. Klankermayer, R. Fröhlich, F. Gumy, J.-C. G. Bünzli, *Chem. Commun.* **2007**, *123*, 1834 – 1836.
[14] G. S. Kottas, M. Mehlstäubl, R. Fröhlich, L. De Cola, *Eur. J. Inorg. Chem.* **2007**, 3465 – 3468.
[15] N. Dannenbauer, K. Müller-Buschbaum, *Z. Anorg. Allg. Chem.* **2013**, *639*, 2737 – 2740.
[16] J.-J. Jiang, L. Li, M.-H. Lan, M. Pan, A. Eichhöfer, D. Fenske, C.-Y. Su, *Chem. Eur. J.* **2010**, *16*, 1841 – 1848.
[17] G. W. Rabe, B. Rhatigan, J. A. Golen, A. L. Rheingold, *Acta Crystallogr.* **2003**, *E59*, m99 – m101.
[18] W. J. Evans, G. W. Rabe, J. W. Ziller, *Inorg. Chem.* **1994**, *33*, 3072 – 3078.
[19] R. Wietzke, M. Mazzanti, J.-M. Latour, J. Pecaut, P.-Y. Cordier, C. Madic, *Inorg. Chem.* **1998**, *37*, 6690 – 6697.
[20] U. P. Singh, S. Tyagi, C. L. Sharma, H. Görner, T. Weyhermüller, *J. Chem. Soc., Dalton Trans.* **2002**, 4464 – 4470.
[21] A. F. Kirby, D. Foster, F. S. Richardson, *Chem. Phys. Lett.* **1983**, *95*, 507 – 512.
[22] W. M. Azevedo, E. A. Gouveia, G. F. De Sa, *J. Lumin.* **1982**, *26*, 337 – 343.
[23] G. Linger, R. Mohan, S. Knittel, G. Duportail, *Spectrochim. Acta, Part A* **1990**, *46*, 797 – 802.
[24] H.-G. Liu, K. Jang, X.-S. Feng, C. Kim, Y.-J. Yoo, Y.-I. Lee, *Bull. Korean Chem. Soc.* **2005**, *26*, 1969 – 1974.
[25] R. A. Sa Ferreira, S. S. Nobre, C. M. Granadeiro, H. I. S. Nogueira, L. D. Carlos, O. L. Malta, *J. Lumin.* **2006**, *121*, 561 – 567.
[26] C. J. Höller, P. R. Matthes, M. Adlung, C. Wickleder, K. Müller-Buschbaum, *Eur. J. Inorg. Chem.* **2012**, 5479 – 5484.
[27] C. J. Höller, M. Mai, C. Feldmann, K. Müller-Buschbaum, *Dalton Trans.* **2010**, *39*, 461 – 468.
[28] P. R. Matthes, C. J. Höller, M. Mai, J. Heck, S. J. Sedlmaier, S. Schmiechen, C. Feldmann, W. Schnick, K. Müller-Buschbaum, *J. Mater. Chem.* **2012**, *22*, 10179 – 10187.
[29] G. H. Dieke, *Spectra and Energy Levels of Rare Earth Ions in Crystals*, Wiley Interscience, New York, **1968**.
[30] G. Blasse, B. C. Grabmaier, *Luminescent Materials*, Springer-Verlag, Berlin, **1994**.
[31] L. Bouscasse, D. Bouin-Roubaud, T. Avignon, *J. Chem. Phys.* **1981**, *75*, 5759 – 5763.
[32] G. Jantsch, H. Jawurek, N. Skalla, H. Gawalowski, *Z. Anorg. Allg. Chem.* **1932**, *207*, 353 – 367.
[33] J. V. de Mello, H. F. Wittmann, R. H. Friend, *Adv. Mater.* **1997**, *9*, 230 – 232.
[34] R. K. Datta, *J. Electrochem. Soc.* **1967**, *114*, 1137 – 1142.
[35] B. M. J. Smets, *Mater. Chem. Phys.* **1987**, *16*, 283 – 299.
[36] SMART, Area Detector Control Software, Bruker Analytical X-ray Instruments Inc., Madison, Wisconsin (USA) **2001**.
[37] XPREP (version 2008/2), Program for symmetry analysis and data reduction of diffraction experiments, Bruker Analytical X-ray Instruments Inc., Madison, Wisconsin (USA) **2008**.
[38] G. M. Sheldrick, *Acta Crystallogr.* **2008**, *A64*, 112 – 122.
[39] O. V. Dolomanov, L. J. Bourhis, R. J. Gildea, J. A. K. Howard, H. Puschmann, *J. Appl. Crystallogr.* **2009**, *42*, 339 – 341.
[40] A. L. Spek, *J. Appl. Crystallogr.* **2003**, *36*, 7 – 13.